Int. J. Solids Structures, 1972, Vol. 8, pp. 347 to 367. Pergamon Press. Printed in Great Britain

BUCKLING ANALYSIS FOR STRUCTURAL SECTIONS AND STIFFENED PLATES REINFORCED WITH LAMINATED COMPOSITES†

A. V. VISWANATHAN,‡ TSAI-CHEN SOONG§|| and R. E. MILLER, JR.¶

The Boeing Company, Seattle, Washington

Abstract—A classical buckling analysis is developed for stiffened, flat plates composed of a series of linked flat plate and beam elements. Plates are idealized as multilayered orthotropic elements; structural beads and lips are idealized as beams. The loaded edges of the stiffened plate are simply supported and the conditions at the unloaded edges can be prescribed arbitrarily. The plate and beam elements are matched along their common junctions for displacement continuity and force equilibrium in an exact manner. Offsets between elements are considered in the analysis. Buckling under uniaxial compressive load for plates, sections and stiffened plates is investigated. Buckling loads are found as the lowest of all possible general and local failure modes and the mode shape is used to determine whether buckling is a local or general instability. Numerical correlations with existing analysis and test data for plates, sections and stiffened plates including boron-reinforced structures are discussed. In general, correlations are reasonably good.

NOTATION

a, b	length and width of plate, Fig. 1
A_b	cross sectional area of beam
$E_{11}, E_{22}, G_{12}, G_{23}$	orthotropic modulus of elasticity, equation (2)
h_k	distance of the kth layer to the reference plane, Fig. 1
h'_k	distance of kth layer to the neutral plane, Fig. 1
I_{xx}, I_{yy}, I_{zz}	moment of inertias of beam about x, y and z axes
J	torsional constant of beam
l	total number of layers of a laminated plate, equation (3)
m	half-wave number in the axial direction
M_{11}, M_{12}, M_{22}	moments, equation (5)
N_{11}, N_{22}, N_{12}	stress resultants, equation (4)
$\bar{N}_{11}$	axial in-plane buckling load, lb/in.
p_i	parameter, equation (13)
P_b, q_y, q_z	loads on beam, Fig. 2
Q^k_{11}, Q^k_{22}, etc.	orthotropicity constants, equation (2)
$\{R_1\}, \{R_2\}$	displacement matrices, equations (32a) and (40)
S^k_{11}	element (1, 1) of matrix $[Q_{ij}]^{-1}$, equation (3)
t_k	thickness of kth layer, Fig. 1
$[T]$	transformation matrix, equations (32a)
T_x	torque on beam, equation (22)
u, v, w	displacements of the neutral plane of a plate or beam
ν_{12}, ν_{21}	Poisson's ratios of orthotropic plate, equation (2)
W, U, V, θ	displacements constants of beam, equation (28)
x, y, z	local coordinates, Fig. 2
y_0, z_0	distances of offset in y and z directions, Fig. 2
z_n	distance of neutral axis of laminated plate, equation (3)

† This work was supported by NASA contract NASI-8858 awarded to the Boeing Company.

‡ Specialist, Structures Staff, Commercial Airplane Group.
§ Senior Specialist, Structures Staff, Commercial Airplane Group.
|| Now at: Xerox Corporation, Rochester, New York.
¶ Head, Stress Analysis Research, Structures Staff, Commercial Airplane Group.

$[\ ]$, $\{\ \}$, $\Gamma\ \ \lrcorner$	rectangular (or square), column and diagonal matrices
$(\ )_{,x}$	$\partial(\ )/\partial x$
α, β	wave-mode parameter, equation (13)
$\sigma_x, \sigma_y, \sigma_{xy}$	in-plane stress components, equation (1)
$\bar{\sigma} I_p$	beam property, equation (22)
Γ	warping constant, equation (22)
ψ	angle between global and local coordinates, Fig. 2
Superscripts	
k	numbering of lamina layers
$\pm$	quantities related to side of plate at $y = \pm b/2$
Subscripts	
BG	quantity belongs to *b*eam element, global coordinates
BS	quantity belongs to *b*eam element, local coordinates
PG	quantity belongs to *p*late element, global coordinates
PS	quantity belongs to *p*late element, local coordinates
G	refer to global coordinates
(1), (2), etc.	element numbers, Fig. 2
i	numbering of characteristic roots
s	refer to offset center *S*, Fig. 2
u, *v*, *w*	along directions of *x*, *y* and *z*, respectively

1. INTRODUCTION

THERE have been numerous publications on general and local instabilities of structure components under axial compression that are made of flat plates and beam-like elements. To cite a few, Ramberg and Levy [1] studied open section extrusions in which local instability was estimated by buckling of flanges taken as plates with suitable edge conditions and general instability analyzed by treating the extrusion as a column. Similar approximations were used in Goodman and Boyd [2] and Goodman's [3] studies of bulb-reinforced flanges. For structural sections, such as *Z*, *T*, channels and hat-type sections, and isotropic plates stiffened by such sections, a usual practice of analysis is to treat them as an assemblage of flat plate elements connected rigidly along the straight boundaries with each element having the same sinusoidal axial mode. The plate is usually taken as infinitely wide and the constraints on its sides are then neglected.

Since a thin plate is rather stiff in the in-plane directions, the common junction between two plate elements can be taken approximately as simply supported as far as lateral displacement is concerned. This simplification reduces analytical work considerably and makes possible some approximate solutions such as moment-distribution [4]. However, when this simple-support assumption is removed, one need not only consider the lateral displacements at the junction, but also the in-plane motions thereof induced by buckling. It is possible to derive, in this rigorous manner, a unified approach for a buckling analysis of structures composed of plate elements which need not distinguish between the so-called local modes and the general modes. The unified approach which seems to be the most exact at the present stage of development can be represented, for example, by Wittrick's papers [5, 6]. Some analyses of similar nature but with various degrees of exactness and generality can be seen in Refs. [7–11].

The present analysis brings the research on stiffened plates and sections another step forward. Here the flat plate element and the beam element that is used to represent beams, lips and beads of flanges, have been extended to unidirectional, laminated composites which, of course, include isotropic material as a particular case. The theory assumes that

the orthotropic physical properties of each layer of the composites are given, i.e. E_{11}, E_{22}, G_{12}, ν_{12} and ν_{21} ($\nu_{21} = \nu_{12}E_{22}/E_{11}$), and the usual Kirchhoff–Love assumption regarding plane sections is valid. Lips and beads of a flange are regarded as beams elastically attached to the side of the flange, and the coupling between axial load and the curvature change is neglected. If the bead is composite reinforced, its physical properties are calculated in an approximate manner. Effect of residual stress due to bonding which may cause prestresses and initial deformations is neglected in the analysis.

Since in most cases where fiber reinforced composites are being used as reinforcements in structural sections, the direction of the fiber runs in the same direction as the axis of the section, the stress–strain equations used in the analysis are restricted to this type of orthotropicity. This simplification, which does not limit the generality of the present theory, reduces greatly the complexity of algebraic manipulations in the analysis as well as in the computer programs. If one needs to accommodate thermal effects and arbitrarily inclined laminated composites in the analysis, he need only use the appropriate stress–strain relationships in the beginning of the derivations. These equations are available in existing literature, for example, Refs. [12, 13].

In the ensuing analysis, elastic instability under uniaxial compression on composite reinforced plates, structural sections reinforced by composites and beaded stiffeners, and finally, stiffened plates reinforced by composites were studied. Buckled shapes from eigenvector solutions were calculated which can be used to ascertain local and general type buckling modes. The analysis and the associated computer programs [14] were correlated with existing analytical and test results, and particularly from the new test data by Boeing [14, 15], of plates, structural sections and stiffened plates reinforced with boron composite laminates. The correlations are reasonably good.

2. BASIC EQUATIONS

In order that readers may be spared from looking for references, possibly with different notations, some of the well-known equations are repeated here for clarity. However, since beams of laminated nature and off-set matching between eccentric elements will soon be introduced into the analysis, these repetitions will not be numerous.

(a) *Equations for composite-laminated flat plate elements*

For an orthotropic lamina, the stress–displacement equations are given by [13]:

$$\begin{Bmatrix} \sigma_x^k \\ \sigma_y^k \\ \sigma_{xy}^k \end{Bmatrix} = [Q_{ij}^k]\{\varepsilon\} = \begin{bmatrix} Q_{11}^k & Q_{12}^k & 0 \\ Q_{12}^k & Q_{22}^k & 0 \\ 0 & 0 & Q_{66}^k \end{bmatrix} \begin{Bmatrix} u_{,x} - zw_{,xx} \\ v_{,y} - zw_{,yy} \\ u_{,y} + v_{,x} - 2zw_{,xy} \end{Bmatrix} \tag{1}$$

where the superscript k denotes lamina number and the elastic constants are:

$$\begin{aligned} (Q_{11}^k, Q_{22}^k) &= (E_{11}, E_{22})/(1 - \nu_{21}\nu_{12}) \\ Q_{12}^k &= \nu_{21}E_{11}/(1 - \nu_{21}\nu_{12}) = \nu_{12}E_{22}/(1 - \nu_{21}\nu_{12}) \\ Q_{66}^k &= G_{12}. \end{aligned} \tag{2}$$

The x, y and z axes for the present orthotropic plate are assumed to be identical with the principle directions of the laminates 1, 2 and 3, respectively as shown in Fig. 1. A distance z_n locates the neutral plane with respect to an arbitrary reference plane. This neutral plane is determined by calculating the resultant of the uniaxial forces in the laminas for a constant and uniform strain across the thickness.

Thus,

$$z_n = \left[\sum_{k=1}^{l} (t_k/2S_{11}^k)(h_{k+1}+h_k)\right] \Big/ \left(\sum_{k=1}^{l} t_k/S_{11}^k\right) \tag{3}$$

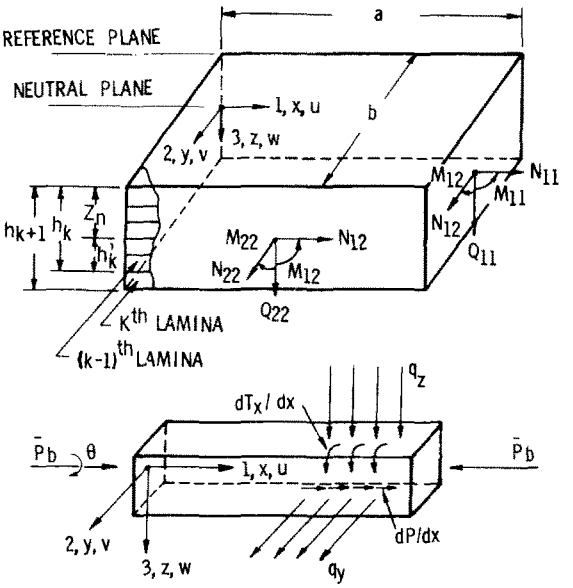

FIG. 1. Sign conventions and coordinates of a laminated plate element and a beam element.

where S_{11}^k is the first element of the matrix $[Q_{ij}^k]^{-1}$, where $[Q_{ij}^k]$, being associated with the kth lamina, is given in equation (1).

From equation (1), integration over the lamina thicknesses, the stress resultants and moments in the neutral plane of the plate can be expressed in u, v and w:

$$\begin{Bmatrix} N_{11} \\ N_{22} \\ N_{12} \end{Bmatrix} = [A_{ij}] \begin{Bmatrix} u_{,x} \\ v_{,y} \\ u_{,y}+v_{,x} \end{Bmatrix} - [B_{ij}] \begin{Bmatrix} w_{,xx} \\ w_{,yy} \\ 2w_{,xy} \end{Bmatrix} \tag{4}$$

$$\begin{Bmatrix} M_{11} \\ M_{22} \\ M_{12} \end{Bmatrix} = [B_{ij}] \begin{Bmatrix} u_{,x} \\ v_{,y} \\ u_{,y}+v_{,x} \end{Bmatrix} - [D_{ij}] \begin{Bmatrix} w_{,xx} \\ w_{,yy} \\ 2w_{,xy} \end{Bmatrix} \tag{5}$$

where the elements of the matrices A, B and D are given by:

$$(A_{ij}, B_{ij}, D_{ij}) = \sum_{k=1}^{l} Q_{ij}^{k} t_k (1, h'_{k+1} + h'_k)/2, \qquad (h'^2_{k+1} + h'_{k+1} h'_k + h'^2_k)/3 \tag{6-8}$$

where the distance h'_k is shown in Fig. 1.

The equilibrium equations for a plate under compression $\bar{N}_{11}$ along x are:

$$N_{11,x} + N_{12,y} = 0, \qquad N_{22,y} + N_{12,x} = 0 \tag{9, 10}$$

$$M_{11,xx} + M_{22,yy} + 2M_{12,xy} - \bar{N}_{11} w_{,xx} = 0. \tag{11}$$

The neutral plane displacements are assumed as:

$$(w, u, v) = \sum_{i=1}^{8} (W_i \sin \alpha, W_i L_{ui} \cos \alpha, W_i L_{vi} \sin \alpha)\, e^{\beta_i} \tag{12}$$

where α is associated with an arbitrary axial half-wave number m and β is a function of the roots p_i of the characteristic equation given in equation (16), and

$$\alpha = m\pi x/a \qquad \beta_i = p_i \pi y/a. \tag{13}$$

Substitution of equations (12) into equations (9)–(11), with the aid of equations (4), (5), yields

$$\begin{bmatrix} R_{11} & R_{12} & R_{13} \\ R_{21} & R_{22} & R_{23} \\ R_{31} & R_{32} & R_{33} \end{bmatrix} \begin{Bmatrix} L_{ui} \\ L_{vi} \\ 1 \end{Bmatrix} W_i = 0 \tag{14}$$

where

$$\begin{aligned} R_{11} &= -A_{11} m^2 + A_{66} p_i^2, \qquad R_{12} = -R_{21} = (A_{12} + A_{66}) m p_i \\ R_{13} &= -R_{31} \pi/a = [B_{11} m^3 - (B_{12} + 2B_{66}) m p_i^2](\pi/a) \\ R_{22} &= A_{22} p_i^2 - A_{66} m^2, \qquad R_{23} = R_{32} = [(B_{12} + 2B_{66}) m^2 p_i^2 - B_{22} p_i^3](\pi/a) \\ R_{33} &= [-\bar{N}_{11} (ma/\pi)^2 + D_{11} m^4 - (2D_{12} + 4D_{66}) m^2 p_i^2 + D_{22} p_i^4](\pi/a)^2. \end{aligned} \tag{15}$$

Expanding the determinant of equation (14), one obtains the characteristic equation:

$$K_8 p_i^8 + K_6 p_i^6 + K_4 p_i^4 + K_2 p_i^2 + K_0 = 0. \tag{16}$$

Equation (16) yields eight roots of p_i, in which four roots are the negative of the other four.

The amplitude ratios L_{ui} and L_{vi} in equation (12) can be obtained from equation (14):

$$L_{ui} = \frac{R_{13} R_{22} - R_{23} R_{12}}{R_{21} R_{12} - R_{22} R_{11}} \qquad L_{vi} = \frac{R_{23} R_{11} - R_{13} R_{21}}{R_{12} R_{21} - R_{22} R_{11}} \qquad i = 1.2.\cdots 8. \tag{17}$$

At a boundary of y constant, Fig. 1, the four displacement quantities ($\theta = w_{,y}$) and the four stress resultants can be found ($Q_{22} = M_{22,y} + 2M_{12,x}$) as:

$$\begin{Bmatrix} w, Q_{22} \\ u, N_{22} \\ v, N_{12} \\ \theta, M_{22} \end{Bmatrix} = \sum_{i=1}^{8} W_i \, e^{\beta_i} \begin{Bmatrix} \sin\alpha, & (q_{22})_i \sin\alpha \\ L_{ui}\cos\alpha, & (n_{22})_i \sin\alpha \\ L_{vi}\sin\alpha, & (n_{12})_i \cos\alpha \\ (\pi p_i/a)\sin\alpha, & (m_{22})_i \sin\alpha \end{Bmatrix} \tag{18, 19}$$

where the quantities related to the stress resultants are given by:

$$\begin{aligned}
(q_{22})_i &= [-B_{12} m p_i L_{ui} + B_{22} L_{vi} p_i^2 + D_{12} m^2 p_i \pi/a - D_{22} p_i^3 \pi/a \\
&\quad - 2B_{66}(m p_i L_{ui} + m^2 L_{vi}) + 4D_{66} m_2 p_i \pi/a](\pi/a)^2 \\
(n_{22})_i &= [-A_{12} m L_{ui} + A_{22} p_i L_{vi} + (B_{12} m^2 - B_{22} p_i^2)(\pi/a)](\pi/a) \\
(n_{12})_i &= [A_{66}(p_i L_{ui} + m L_{vi}) - 2B_{66} p_i m \pi/a](\pi/a) \\
(m_{22})_i &= [-B_{12} L_{ui} m + B_{22} L_{vi} p_i + (D_{12} m^2 - D_{22} p_i^2)(\pi/a)](\pi/a).
\end{aligned} \tag{20}$$

(b) *Equations for laminated beam elements*

Beads or lips in structural sections, beam-type boron reinforcements and joints with fillets, such as corners of extruded structural sections, may be idealized as beams. Origin of coordinates of the cross section is chosen, for convenience, at the geometric center of the section. The basic material properties involved are the individual lamina constants, such as E_{11}^k and G_{23}^k for the kth layer.

The equilibrium equations for the laminated beams are derived from elementary beam theory. Consider a beam subjected to a constant axial loading $\bar{P}_b$ (see Fig. 1) and is connected to the side of a plate. Due to the displacements of the plate, the elastic loads acting along the neutral axis of the beam can be expressed by the displacements u, v, w and rotation θ of the axis and the external constant loading $\bar{P}_b$. These equations are:

$$q_z = E_{11} I_{yy}(\mathrm{d}^4 w/\mathrm{d}x^4) + \bar{P}_b(\mathrm{d}^2 w/\mathrm{d}x^2) \tag{21}$$

$$\mathrm{d}T_x/\mathrm{d}x = E_{11}\Gamma(\mathrm{d}^4\theta/\mathrm{d}x^4) - (G_{23}J - \bar{\sigma}I_p)(\mathrm{d}^2\theta/\mathrm{d}x^2) \tag{22}$$

$$\mathrm{d}P/\mathrm{d}x = -E_{11} A_b(\mathrm{d}^2 u/\mathrm{d}x^2) \tag{23}$$

$$q_y = E_{11} I_{zz}(\mathrm{d}^4 v/\mathrm{d}x^4) + \bar{P}_b(\mathrm{d}^2 v/\mathrm{d}x^2) \tag{24}$$

where θ of the beam is assumed to be the same as $w_{,y}$ at the edge of the plate.

The stiffness quantities required in these equations are calculated in an approximate manner as follows:

$$E_{11}F = \sum_{k=1}^{l} E_{11}^k F^k \tag{25}$$

where F denotes I_{yy}, I_{zz}, Γ or A_b (I_{xx}^k and I_{yy}^k are moments of inertia of kth lamina about the neutral axis of the beam). The torsion constants are

$$G_{23}J - \bar{\sigma}I_p = \sum_{k=1}^{l} (G_{23}^k J^k - \bar{\sigma}^k I_p^k) \tag{26}$$

where the applied stress in the kth lamina, denoted by $\bar{\sigma}^k$, is calculated on the assumption that the axial strain is the same in all laminas. The expression for $G_{23}J$ as given in equation (26) is appropriate for beams whose cross sections are made of concentric circular layers or concentric rectangular box-type layers. However, it should not be used for beams whose section is rectangular and composed of layered thin plates, since such laminas shall deform with different eccentricities towards the shear center of the overall section of the beam. In lacking an exact torsional stiffness expression for layered composite rectangular sections, the following approximate equation has been used:

$$G_{23}J = \left[\left(\sum_{k=1}^{l} G_{23}^k A_b^k\right) \Big/ \left(\sum_{k=1}^{l} A_b^k\right)\right] (J_{\text{overall section}}) \tag{27}$$

where A_b^k is the cross sectional area of the kth layer. Physical properties of these circular and rectangular cross section beams can be found in Refs. [1, 14, 16, 17].

The buckling displacements are assumed as

$$(w, \theta, u, v) = (W \sin \alpha, \theta \sin \alpha, U \cos \alpha, V \sin \alpha) \tag{28}$$

where α is equal to $m\pi x/a$ as given in equation (13). These displacements satisfy the simply supported conditions at $x = 0$ and $x = a$ where the external compressive force is applied.

Substitution of equation (28) into equations (21)–(24) yields

$$\begin{aligned} q_z &= W[E_{11}I_{yy}(m\pi/a)^4 - \bar{P}_b(m\pi/a)^2] \sin \alpha = W\xi_1 \sin \alpha \\ \mathrm{d}T_x/\mathrm{d}x &= \theta[E_{11}\Gamma(m\pi/a)^4 + (G_{12}J - \bar{\sigma}I_p)(m\pi/a)^2] \sin \alpha = \theta\xi_2 \sin \alpha \\ \mathrm{d}P/\mathrm{d}x &= U[E_{11}A_b(m\pi/a)^2] \cos \alpha = U\xi_3 \cos \alpha \\ q_y &= V[E_{11}I_{zz}(m\pi/a)^4 - \bar{P}_b(m\pi/a)^2] \sin \alpha = V\xi_4 \sin \alpha. \end{aligned} \tag{29}$$

Since the beam element is continuously attached to a plate element to form a stiffener, the boundary conditions applicable to all beam elements are:

$$(q_z, \mathrm{d}T_x/\mathrm{d}x, \mathrm{d}P/\mathrm{d}x, q_y) = (\mp Q_{22}, \pm M_{22}, \mp N_{12}, \mp N_{22}) \tag{30}$$

where the right-hand side quantities are given in equations (19); and the upper and lower sets of signs are for the beam to be connected to the plate at $y = 0$ and $y = b$, respectively (Fig. 1).

(c) *Transformations of plate equations and beam equations*

Figure 2 shows an idealized eight-element structure where the dash-line configuration is the cross-section of the structure and the solid lines are the neutral planes. Elements (6) and (8) are chosen to illustrate conventions for the local and global axes. Forces and displacements of element (6) at end point B shall be transformed to point S and transformed further into global coordinates for matching with neighboring element. The offsets y_0 and z_0 are measured along the positive directions of the local axes. The following are the

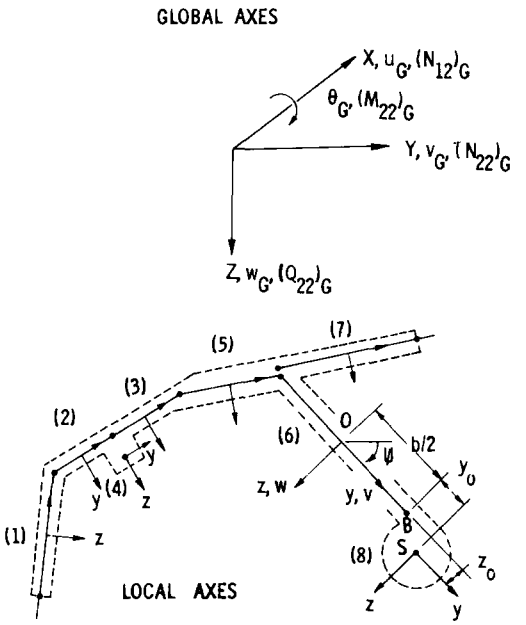

FIG. 2. Idealization of an eight-element panel and sign conventions of global and local coordinates.

approximate displacement relationships between points S and B:

$$\begin{aligned} w_s &= w + y_0 w_{,y} = w + y_0\theta \\ \theta_s &= (w_{,y})_s = w_{,y} = \theta \\ u_s &= u - \underline{z_0 w_{,x}} - \underline{y_0 v_{,x}} \\ v_s &= v - z_0 w_{,y} = v - z_0\theta. \end{aligned} \tag{31}$$

The transfer is a rigid-body motion in three planes when the underlined terms are omitted. With the underlined terms included, the effect on u-displacement change at S due to curvatures $w_{,x}$ and $v_{,x}$ in the line passing through B can be included. Physically, this means that there is no relative slippage between B and S along the x-axis. The effect might be significant when S is the centerline of a deep beam or a thick plate with large offsets z_0 and y_0. Similar terms are also underlined in equations (34) and (37).

Substitution of equations (18) into (31) and making a coordinate transformation, one obtains the global displacements for the plate ($B_{ij} \neq 0$):

$$\begin{Bmatrix} w_G \\ \theta_G \\ u_G \\ v_G \end{Bmatrix} = [T] \begin{bmatrix} [1 + y_0(\pi p_i/a)]\, e^{\beta_i} \sin\alpha \\ (\pi p_i/a)\, e^{\beta_i} \sin\alpha \\ [L_{ui} - (m\pi/a)(z_0 + y_0 L_{vi})]\, e^{\beta_i} \cos\alpha \\ [L_{vi} - z_0(\pi p_i/a)]\, e^{\beta_i} \sin\alpha \end{bmatrix}_{i=1,2,\ldots,8} \{R_1\} \tag{32}$$

where the coordinate transformation matrix $[T]$ and the column matrix $\{R_1\}$ are:

$$[T] = \begin{bmatrix} \cos\psi & 0 & 0 & \sin\psi \\ 0 & 1 & 0 & 0 \\ 0 & 0 & 1 & 0 \\ -\sin\psi & 0 & 0 & \cos\psi \end{bmatrix}, \qquad \{R_1\} = \begin{Bmatrix} W_1 \\ W_2 \\ \vdots \\ W_8 \end{Bmatrix}. \tag{32a}$$

In the following text, superscripts + and − will be used with some matrices to distinguish the quantity y of β_i in the matrix according to $y = +b/2$ or $y = -b/2$, respectively. Thus, displacements at the two sides can be written generally as:

$$\{d_{PG}^{\pm}\} = [T][X_1^{\pm}]\{R_1\} = [X_3^{\pm}]\{R_1\}, \qquad y = \pm b/2 \text{ in } \beta_i \text{ of } [X_1^{\pm}]. \tag{33}$$

In a similar manner, the forces along the side $y = +b/2$ when transferred to a parallel line through S, becomes

$$\begin{aligned} (Q_{22})_s &= Q_{22} - \underline{z_0 N_{12,x}} \\ (M_{22})_s &= M_{22} + y_0 Q_{22} - z_0 N_{22} \\ (N_{12})_s &= N_{12} \\ (N_{22})_s &= N_{22} - \underline{y_0 N_{12,x}}. \end{aligned} \tag{34}$$

With substitution of equations (19) to equations (34) and making a transformation into global axis, with $\pm[T]$ used for matching at $y = \pm b/2$, respectively, one obtains

$$\begin{Bmatrix} (Q_{22})_G \\ (M_{22})_G \\ (N_{12})_G \\ (N_{22})_G \end{Bmatrix} = \pm[T] \begin{bmatrix} [(q_{22}) + z_0(n_{12})_i(m\pi/a)]\, e^{\beta_i} \sin\alpha \\ [(m_{22})_i + y_0(q_{22})_i - z_0(n_{22})_i]\, e^{\beta_i} \sin\alpha \\ (n_{12})_i\, e^{\beta_i} \cos\alpha \\ [(n_{22})_i + y_0(n_{12})_i(m\pi/a)]\, e^{\beta_i} \sin\alpha \end{bmatrix}_{i=1,2,\ldots,8} \{R_1\} \tag{35}$$

which can be written in a matrix form as:

$$\{f_{PG}^{\pm}\} = \pm[T][X_2^{\pm}]\{R_1\} = [X_4^{\pm}]\{R_1\}, \qquad y = \pm b/2 \text{ in } \beta_i \text{ of } [X_2^{\pm}]. \tag{36}$$

For the case of $B_{ij} = 0$, corresponding equations can be found in Ref. [15].

Similarly, for the beam elements, the displacements and forces at a point B transferred to a point S with offsets y_0 and z_0 (Fig. 2) are expressed by:

$$\begin{aligned} w_s &= w + y_0\theta & (q_z)_s &= q_z + \underline{z_0(\mathrm{d}^2P/\mathrm{d}x^2)} \\ \theta_s &= \theta & (\mathrm{d}T_x/\mathrm{d}x)_s &= \mathrm{d}T_x/\mathrm{d}x + z_0 q_y - y_0 q_z \\ u_s &= u - \underline{z_0 w_{,x}} - \underline{y_0 v_{,x}} & (\mathrm{d}P/\mathrm{d}x)_s &= \mathrm{d}P/\mathrm{d}x \\ v_s &= v - z_0\theta & (q_y)_s &= q_y + \underline{y_0(\mathrm{d}^2P/\mathrm{d}x^2)}. \end{aligned} \tag{37}$$

Substitution of equations (28) and (29) into (37) and making a coordinate transformation lead to corresponding equations in global coordinates with offsets included:

$$\{d_{BG}\} = [T][X_5]\{R_2\} = [X_7]\{R_2\} \tag{38}$$

$$\{f_{BG}\} = [T][X_6]\{R_2\} = [X_8]\{R_2\} \tag{39}$$

where $\{d_{BG}\}$ and $\{f_{BG}\}$ have the same expressions as the left-hand sides of equations (32) and (35), respectively, and the two square matrices and the column matrix are given by:

$$[X_5] = \begin{bmatrix} 0 & 0 & \sin\alpha & y_0 \sin\alpha \\ 0 & 0 & 0 & \sin\alpha \\ \cos\alpha & -y_0\frac{m\pi}{a}\cos\alpha & -z_0\frac{m\pi}{a}\cos\alpha & 0 \\ 0 & \sin\alpha & 0 & -z_0\sin\alpha \end{bmatrix} \quad \{R_2\} = \begin{Bmatrix} U \\ V \\ W \\ \theta \end{Bmatrix} \tag{40}$$

$$[X_6] = \begin{bmatrix} -z_0\xi_3\frac{m\pi}{a}\sin\alpha & 0 & \xi_1\sin\alpha & 0 \\ 0 & z_0\xi_4\sin\alpha & -y_0\xi_1\sin\alpha & \xi_2\sin\alpha \\ \xi_3\cos\alpha & 0 & 0 & 0 \\ -y_0\xi_3\frac{m\pi}{a}\sin\alpha & \xi_4\sin\alpha & 0 & 0 \end{bmatrix}. \tag{41}$$

This completes equations for matching of plate elements and beam elements with offsets included. The unloaded side of a plate that is not in conjunction with other elements may be free clamped, simple supported or elastically restrained. The forces and displacements can be referred to the neutral plane of the plate in local coordinates. Take the clamped and simple supported cases as examples. From equations (18) and (19), they are, respectively

$$(w, w_{,y}, u, N_{22}) = \sum_{i=1}^{8} W_i\, e^{\beta_i}(1, m\pi/a, L_{ui}, (n_{22})_i) = 0 \tag{42}$$

$$(w, M_{22}, u, N_{22}) = \sum_{i=1}^{8} W_i\, e^{\beta_i}(1, (m_{22})_i, L_{ui}, (n_{22})_i) = 0 \tag{43}$$

which may be written respectively as

$$[X_9^{\pm}]\{R_1\} = 0, \qquad [X_{10}^{\pm}]\{R_1\} = 0 \qquad y = \pm b/2 \text{ in } \beta_i. \tag{44}$$

(d) *Buckling criteria*

The criteria of buckling can be given in terms of critical strain or critical load intensity. For composite reinforced stiffened plate, the critical load per unit length is different for different plate elements for constant axial shortening. The critical strain ε_{cr} is defined as the uniform axial strain ε_x in equation (1) at the instant of buckling such that the orthogonal stress σ_y^k in the kth lamina, and all the other laminas, is zero while the sum of the axial stress σ_x^k, through the thickness of the plate, is equal to the applied uniform line load $\bar{N}_{11}$. Thus,

by inverting equation (1) and putting σ_y^k and σ_{xy}^k equal to zero, one arrives at an expression of the critical strain

$$\varepsilon_{cr} = \varepsilon_x = \bar{N}_{11} \Big/ \left(\sum_{k=1}^{l} (t^k / S_{11}^k) \right). \tag{45}$$

If one assumes that the orthogonal stress resultant N_{22} is zero, instead of lamina stress σ_y^k in each lamina is zero, one arrives at the more familiar equation for orthotropic plate

$$\varepsilon_{cr} = \varepsilon_x = \bar{N}_{11} / (A_{11} - (A_{12}^2 / A_{11})). \tag{46}$$

These two equations will produce the same critical strain criteria, since prebuckling deformations are ignored in the present analysis.

3. STIFFNESS APPROACH

In the previous approach, the matching between neighbouring elements at a junction is based on satisfaction of both forces and displacements. The eigenvectors in the resulting buckling equation are the displacement parameters, $\{R_1\}$ and $\{R_2\}$ of equations (32a) and (40). It has the advantages of a direct, simple derivation, no matrix inversion and is convenient for buckling-mode plots. However, when the structure involves a large number of elements, a smaller buckling determinant is preferred. This can be achieved by further manipulations of the calculated quantities to eliminate the $\{R_1\}$ and $\{R_2\}$ parameters and use the displacement vectors at the junctions as the eigenvectors in the buckling equations. This is the stiffness formulation and will be described simply in the following.

For a plate element which has only one lateral side connected to other elements, the free side can be taken as elastically restrained where the external elastic force (or moments) can be varied from 0 to infinity to simulate a no-force to no-displacement condition. This arrangement permits a single formulation to represent all the classical homogeneous boundary conditions and is very convenient in programming [6].

The spring force vector which is proportional to the displacement vector is given by,

$$\{f_{PG}^{\pm}\} = -\lceil k^{\pm} \rfloor \{d_{PG}^{\pm}\} = -\lceil k^{\pm} \rfloor [X_3^{\pm}] \{R_1\} \tag{47}$$

where the + and − signs in the superscript refer to the free side at $y = +b/2$ and $y = -b/2$, respectively. Thus, for example, $\lceil k^- \rfloor$ is a diagonal matrix for the four spring constants when side $y = -b/2$ is the side not connected to other elements. $[X_3^{\pm}]$ are given in equation (33).

Equating $\{f_{PG}^{\pm}\}$ of equation (47) to that of equations (36) and using equations (33), one can solve for $\{R_1\}$, which, after substitution in equations (36), yields the stiffness matrix:

$$\{f_{PG}^{\mp}\} = [X_4^{\mp}] \begin{bmatrix} [X_4^{\pm}] + \lceil k^{\pm} \rfloor [X_3^{\pm}] \\ [X_3^{\mp}] \end{bmatrix}^{-1} \begin{Bmatrix} 0 \\ --- \\ \{d_{PG}^{\mp}\} \end{Bmatrix} \tag{48}$$

where the upper superscript is used when matching of equilibrium with other elements is done at $y = -b/2$ and the lower superscript is used when matching is at $y = +b/2$.

The stiffness matrices for a plate with both sides to be matched with other elements are:

$$\{f_{PG}^{\pm}\} = [X_4^{\pm}] \begin{bmatrix} X_3^- \\ X_3^+ \end{bmatrix}^{-1} \begin{Bmatrix} d_{PG}^- \\ d_{PG}^+ \end{Bmatrix}. \tag{49}$$

The stiffness matrix for a beam element can be found from equations (38) and (39) as

$$\{f_{BG}\} = [X_8][X_7]^{-1}\{d_{BG}\} \tag{50}$$

Equations (48)–(50) are the required stiffnesses where the nodal displacements form the eigenvectors in the buckling equations.

It is appropriate to note here that because of the additions of the underlined terms in equations (31), (34) and (37), which modified the classical rigid-body transformation between offset nodal lines, there is no slippage along the x direction between offsets. It can be shown that the stiffness matrices thus obtained still maintain the condition of symmetry as is required by the reciprocal theorem for linear elastic systems. In the stiffness approach, the eigenvectors of the buckling determinantal equations are the nodal displacements which is smaller in number than the displacement parameters. Consequently, the final buckling determinant is much smaller in size by using the stiffness approach than the parametric method. However, to derive the buckling mode as based on the nodal displacements, more calculations are required than if the displacement parameters of each element are known. Therefore, both versions have relative advantages.

4. EXAMPLE

The eight-element stiffened plate as shown in Fig. 2 will be used as an example to derive the buckling equations where the deflection parameters are the eigenvectors. For illustrative purpose, assuming that the left- and the right-hand sides of the plate are respectively simply supported and clamped, the previous equations lead to the following simultaneous equations written in a matrix form:

$$\begin{array}{c}
\begin{array}{cccccccc} (1) & (2) & (4) & (3) & (5) & (6) & (7) & (8) \end{array} \\
\begin{bmatrix}
X_{10}^- & & & & & & & \\
X_3^+ & -X_3^- & & & & & & \\
X_4^+ & X_4^- & & & & & & \\
 & X_3^+ & -X_7 & & & & & \\
 & & X_7 & -X_3^- & & & & \\
 & X_4^+ & X_8 & X_4^- & & & & \\
 & & & X_3^+ & -X_3^- & & & \\
 & & & X_4^+ & X_4^- & & & \\
 & & & & X_3^+ & -X_3^- & & \\
 & & & & & X_3^- & -X_3^- & \\
 & & & & X_4^+ & X_4^- & X_4^- & \\
 & & & & & X_3^+ & & -X_7 \\
 & & & & & X_4^+ & & X_8 \\
 & & & & & & X_9^+ &
\end{bmatrix}
\begin{Bmatrix}
R_{1(1)} \\ R_{1(2)} \\ R_{2(4)} \\ R_{1(3)} \\ \\ R_{1(5)} \\ R_{1(6)} \\ R_{1(7)} \\ R_{2(8)}
\end{Bmatrix} = 0
\end{array} \tag{51}$$

where the numbers in parenthesis are the element numbers to which the appropriate quantities belong. The square matrix in equation (51) is the buckling determinant, of order 56×56. A common factor of $\sin \alpha$ and $\cos \alpha$ ($\alpha = m\pi x/a$) should be taken from the rows of the determinant.

For a stiffened plate with a number of repeated sections, only a beginning section, a repeating section and an ending section need to be calculated. Details of such examples are given in Ref. [15].

The buckling load, or the critical strain, which is the lowest eigenvalue in equation (51), corresponding to a given value of m, can be obtained by the usual trial-and-error method. In Ref. [6], a bound method which seems to be a much faster iterative procedure to determine the buckling load has been suggested for symmetric matrix buckling equations derived from the stiffness approach.

5. CORRELATIONS WITH OTHER ANALYTICAL AND TEST RESULTS

In correlation studies with other analytical results, the mathematical model used in others' analyses will be followed, i.e. whether a stiffener is treated as a beam or a plate assembly in the present method will be consistent with those in the corresponding references. All numerical results are obtained by using the displacement-parameter approach.

Figure 3 shows correlation with a simply supported web-flange of local buckling modes studied in Ref. [18] in which the flange is treated as a plate. It can be seen from Fig. 3 that when the section is reinforced on the outstanding flange by composites, the flange seems stiff enough to force a node-line at the junction and the approximate analysis of Ref. [18] which implied such an assumption agrees very well with the present more exact

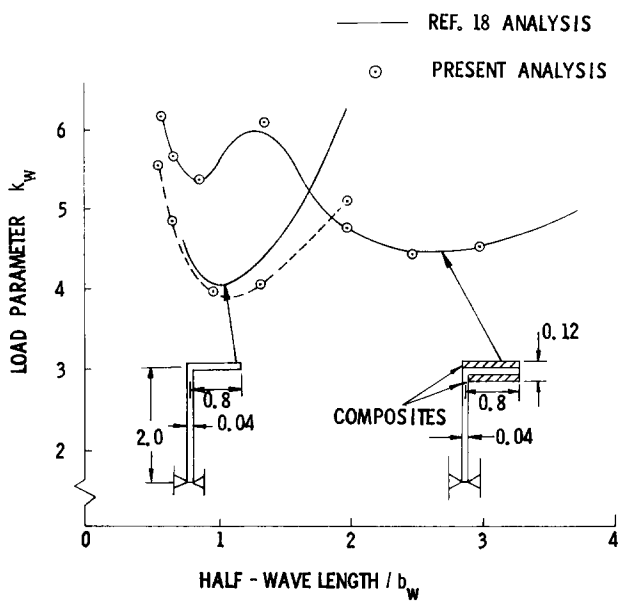

FIG. 3. Buckling of web-flange with and without composite reinforcement at the flange (unit: in.).

method. However, when the flange is not reinforced, the flexibility at the junction made the results of Ref. [18] higher than the present method.

Figure 4 shows seven types of aluminum-alloy multi-stiffened plates and truss-core sandwich panels. The degree of exactness of the analyses in original references varied. In general, translations of the junctions are omitted while force equilibrium of them are maintained. Results of correlations are given in Table 1 which seem to be reasonably good. The higher buckling loads predicted by the present method for panels (6) and (7) are

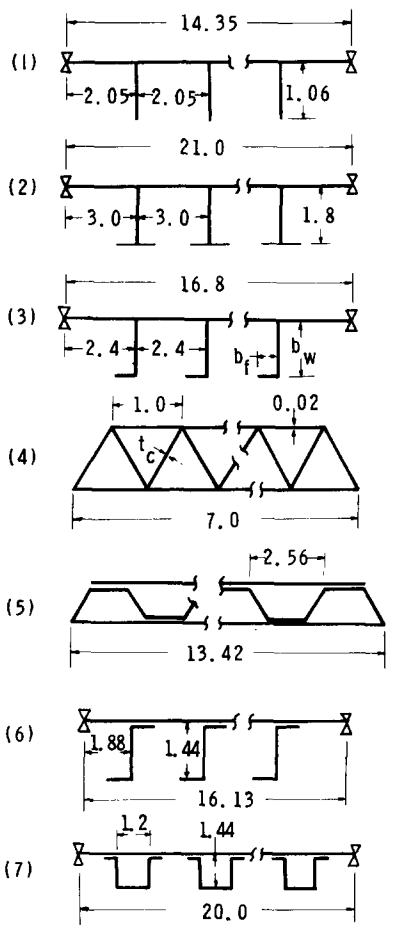

FIG. 4. Shapes and overall dimensions of seven types of isotropically stiffened plates and truss-core panels for analytical correlations (unit: in.).

probably due to the fact that the flanges of the Zee and hat-sections which are in contact with the base plate are considered as an integral part of the base plate in the present analysis while in the references they are taken as separate. The latter resembles a riveted attachment while the former is similar to a bonded connection. It is interesting to note that tests conducted in Ref. [19] showed that the buckling stress of a bonded Zee-section stiffened plate is 19 per cent higher than a corresponding riveted counterpart. Incidentally, this value is quite close to the 18 per cent as indicated by panel 6 of Table 1.

TABLE 1. CORRELATIONS OF ANALYTICAL RESULTS IN LITERATURE AND THE PRESENT METHOD FOR THE SEVEN PANELS SHOWN IN FIG. 4

Panel	No. of stiffeners	Length (in.)	Remarks	Reference	Comparison of Buckling load		
					Reference†	Present method	Ratio
1	6	12·3	Stiffener treated as discrete plate	[20]	$k_s = 1{\cdot}87$	1·86 ($m = 6$)	1·01
			Stiffener treated as smeared beam	[21]	$P_{cr} = 23{,}450$ (1)	22,432 (1)	1·04
2	6	15·0	Local mode, stiffener treated as plate	[20]	$k_s = 4{\cdot}30$	4·25 (5)	1·01
3	6	14·4	Case A: $b_w = 1{\cdot}92$ $b_f = 0{\cdot}576$	[20]	$\sigma_{cr} = 21{\cdot}400$	21,300 (9)	1·01
			Case B: $b_w = 0{\cdot}96$ $b_f = 0{\cdot}288$		$\sigma_{cr} = 42{,}000$	41,600 (6)	1·01
4		6·0	Case A: $t_c = 0{\cdot}02$	[22]	$\sigma_{cr} = 16{,}920$	16,954 (7)	1·00
			Case B: $t_c = 0{\cdot}01$	[22]	$\sigma_{cr} = 6070$	6019 (9)	1·01
5		8·96	Treated as discrete plates	[23]	$\sigma_{cr} = 20{,}400$ (5)	19,550 (5)	1·03
6	6	16·0	Treated as discrete plates	[23]	$\sigma_{cr} = 40{,}900$ (7)	49,800 (12)	0·82
7	5	20·0	Treated as discrete plates	[23]	$\sigma_{cr} = 47{,}700$ (10)	52,500 (17)	0·91

† k_s is a buckling load parameter which is proportional to the buckling load, P_{cr} is the total load, lb. and σ_{cr} is the stress, psi.

For illustration, the buckling shape of the truss-core panel (4) of Fig. 4 is shown in Fig. 5. Results corresponding to two core web thicknesses are presented. It shows clearly that in case A, which has the same core web thickness as the face sheet, the face sheets near the two free edges of the panel buckled; while in case B, the web is thinner than the face, and the core in the center of the panel buckled first. Usefulness of the buckle shape plot to aid design is evident.

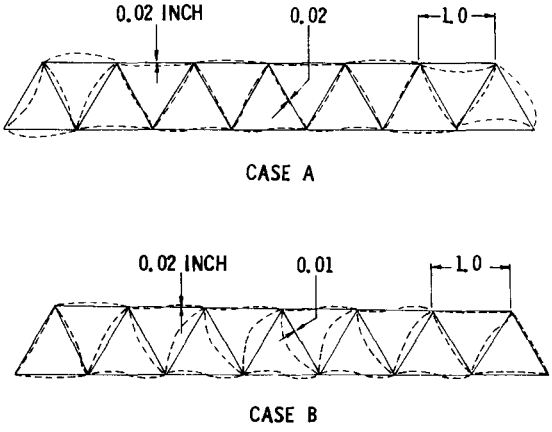

FIG. 5. Buckling shapes of two truss-core sandwich panels with different web thickness: case A, panel 4 in Fig. 4, core-restrains-face type (core web thickness = 0·02); case B, panel 4 in Fig. 4, face-restrains-core type (core web thickness = 0·01). Note: the relative amplitude of each element of the buckled shape is drawn in scale.

In the next paragraphs, correlations are given with available test data on axially compressed plates, sections and stiffened plates reinforced with boron laminated composites.

Boron-reinforced plates

Table 2 shows test correlations for boron-reinforced plates from three sources. In test denoted as (1), from Ref. [24], the specimens are all-composite laminated, 20-ply plates with dimension $11 \times 9{\cdot}95$ in. In test (2), plates are similar, with dimension 10×10 in. In tests (3) by Boeing [15], a total of 48 specimens divided into sixteen groups were tested. Half of the specimens were symmetrically laminated, with titanium layer in the middle and boron laminates on both sides; and the other half specimens were unsymmetrically laminated. Load edges are clamped. The analytical prediction is based on the measured layer thickness of each specimen but the test load and the analysis load as given in Table 2 are the average of the three specimens in each group. The scattering of the test correlations is believed due to less-than-exact boundary constraints and also due to difficulties in interpreting the accurate buckling load from test load–deflection curves.

TABLE 2. TEST CORRELATIONS FOR BORON REINFORCED RECTANGULAR PLATES

Plate No. in Ref.	Composite information	Buckling load (lb/in.) Test	Present analysis	Ratio	Buckling load (lb/in.) Test	Present analysis	Ratio
(1) Tests reported in Ref. [24]		(unloaded edges simply supported)			(unloaded edges free)		
404	Fiber ∥ to load	271	286·5	0·95	199·0	206·5	0·97
405	Fiber ⊥ to load	251	217·0	1·16	23·3	22·6	1·01
(2) Tests reported in Ref. [25]		(load ∥ to 0°-axis)			(load ⊥ to 0°-axis)		
1	0 and 90° alternate	1130	1170	0·97	960	990	1·17
4	Same	740	730	1·01	720	617	1·16
5	All fibers parallel	1240	1210	1·02	435	304	1·43
20	Same	1370	1335	1·03	420	336	1·25
(3) Tests reported in Ref. [15]		(unloaded edges simply supported)			(unloaded edges free)		
8A	Unsymmetrically laminated	3625	3766	0·96	700	799	0·87
8B	Same	3625	4229	0·86	751	925	0·81
8C	Same	3243	3794	0·86	709	843	0·84
8D	Same	4167	4613	0·90	838	1023	0·82
8E	Symmetrically laminated	3805	4433	0·86	1163	1595	0·73
8F	Same	4397	5199	0·85	1317	1778	0·74
8G	Same	4795	5237	0·92	1120	1724	0·65
8H	Same	4082	4432	0·92	1002	1229	0·82

The physical properties of boron composites and titanium used in the analysis for Boeing test specimens are:

TABLE 3

Boron-epoxy BP 907	Titanium 6A1-4V
$E_{11} = 29{\cdot}117 \times 10^6$ psi	$E = 16{\cdot}4 \times 10^6$ psi
$E_{22} = 2{\cdot}341 \times 10^6$ psi	$G = 6{\cdot}2 \times 10^6$ psi
$G = 0{\cdot}75 \times 10^6$ psi	$\nu = 0{\cdot}3$
$\nu_{12} = 0{\cdot}2467$	Density = 0·158 lb/in.^{3}
Density = 0·072 lb/in.^{3}	

Boron reinforced structural sections

Figure 6 shows five types of Boeing test specimens of structural sections. All are titanium except 9G-1 and 9H-1 which are Al alloy, reinforced with unidirectional boron composite strips and rods. Ply thickness is 0·0053 in. and adhesive thickness is 0·018 in. More details are given in Table 4.

These test specimens are machined flat at the loaded edges and placed in the testing machine without any fixtures. Unloaded sides are free. In the analysis, the lips of Z-sections and the tips of T-sections are idealized as beams while all the other reinforced parts are treated as plate elements. Test results and correlations are given in Table 5. Except specimens 9A-1 and 9J-1, correlations are reasonably good.

Boron reinforced stiffened plates

Figure 7 shows the geometry of three types of Boeing test specimens of boron-reinforced stiffened plates. They are free at the parallel sides and machined flat at the ends. Specimens 11-A, -C, -E, -G and -I are long plates of 33·7 in., whose skin is instrumented for elastic skin buckling. Specimens 11-B, -D, -F, -H and -J are short plates of lengths 15·0 in. and tested for ultimate loads with no intention for elastic initial buckling correlation. In the analysis, the deep boron strips in plates -A, -B, -G, -H, -I and -J are treated as beams connected to the two sides of angles, taken as plates; while in -C, -D, -E and -F, the boron strips together with the immediate skins are taken as plate elements. From Table 6, one sees that all the predicted elastic buckling loads are lower than the test ultimate loads, except -E and -F, which are honeycomb sandwich plates whose core was crushed before buckling occurs, and -I, where the two numbers are very close. In general, the correlations are satisfactory. The higher predictions may be due to the fact that the boundaries are restrained against lateral movement by friction only while the analysis assumes no lateral movements.

6. CONCLUSIONS

The present analysis for the instability of composite plates, sections and stiffened plates with composite reinforcements, is an exact theory in the classical sense. The connections

TABLE 4. DETAILS OF GEOMETRY OF STRUCTURAL SECTIONS IN TEST SPECIMENS FIG. 6

Specimen type	Length (in.)	Ply Nos.	t (in.)	t_1 (in.)	b (in.)	b_1 (in.)	r (in.)
9A-1 -1 to -4	12·0	8	0·040		1·16		0·03
-5 to -7	20·0	8	0·040		1·16		0·03
9B-1	13·6	12	0·063		1·10		0·12
9C-1	13·6	12	0·063		1·10		0·12
9D-1 -1 to -4	12·0	8	0·040		1·16		0·08
-5 to -7	20·0	8	0·040		1·16		0·08
9E-1	13·6	12	0·063		0·43	0·28	0·125
9F-1	12·8	5	0·063		0·50	0·50	0·05
9G-1	6·0		0·012				
9H-1	6·0		0·020				
9I-1	10·0	8	0·063	0·125			
9J-1	9·2	3	0·025	0·050			

TABLE 5. TEST CORRELATIONS OF BOEING SPECIMENS OF BORON-REINFORCED STRUCTURAL SECTIONS (FIG. 6)

Specimens†		Average ultimate test load (lb)	Average elastic test buckling load (lb)	Analysis, buckling prediction	
Type	No. tested			Load (lb)	Ratio test/analysis
9A-1	4	8375	3500 (0·0012)‡	2390 (0·00051)‡ (1)§	1·46
	3	5967	2130 (0·0052)	2150 (0·00046) (1)	0·99
9B-1	2	10,170	5900	7010 (0·00098) (1)	0·85
9C-1	3	27,333	19,700 (0·0023)	18,180 (0·0020) (2)	1·08
9D-1	4	9920	5510 (0·0015)	5740 (0·00093) (2)	0·96
	3	11,660	5300 (0·0012)	5660 (0·00092) (3)	0·95
9E-1	1	33,300	33,300 (0·0033)	35,890 (0·0058) (1)	0·93
9F-1	1	6900	4300 (0·0020)	4390 (0·0016) (5)	0·98
9G-1	2	19,700	17,620 (0·0012)	18,870 (0·0017) (1)	0·93
9H-1	3	21,520	21,520 (0·0073)	23,520 (0·0041) (1)	0·92
9I-1	4	37,700	28,250 (0·0043)	28,830 (0·0041) (1)	0·98
9J-1	3	10,910	2270 (0·00085)	1850 (0·00067) (1)	1·23

† All test specimens are titanium except 9G-1 and 9H-1 which are aluminum.
‡ Unit strain, in./in.
§ Axial half-wave number.

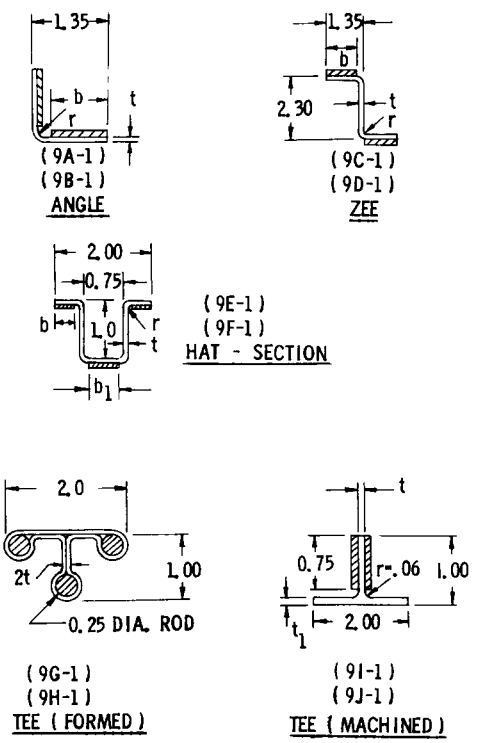

FIG. 6. Cross-section geometry of test specimens of boron-reinforced titanium or aluminum alloy structural sections. Materials given in Table 5. Ply thickness of boron tape = 0·0053 in. (nominal). Adhesive thickness = 0·018 approx.

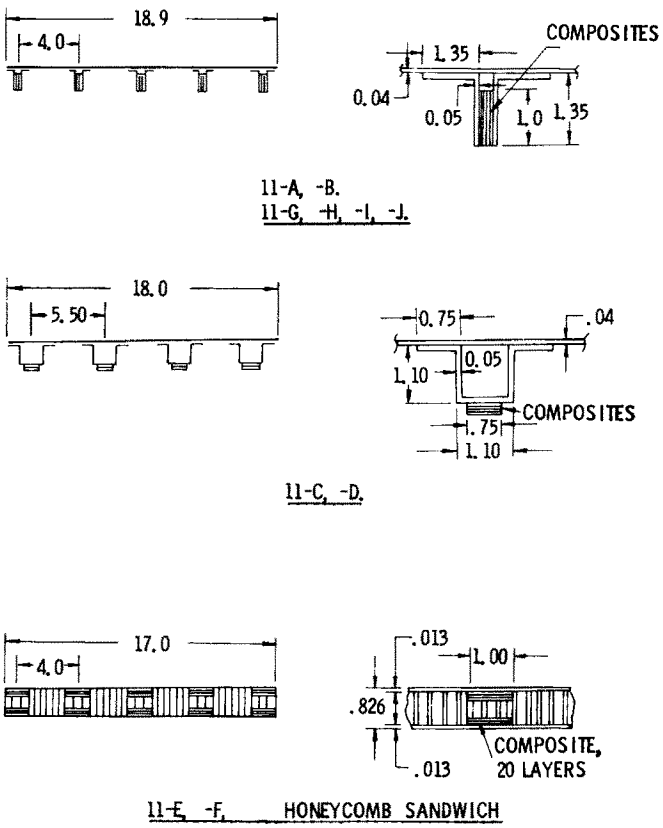

FIG. 7. Cross-section geometry of test specimens for boron composite reinforced stiffened plates and stiffened honeycomb-sandwich panel (unit: in.). Thickness of each boron tape layer = 0·0053 in. Thickness of adhesive layer = 0·013 in. approx.

TABLE 6. TEST CORRELATIONS OF BOEING SPECIMENS OF BORON-REINFORCED STIFFENED PLATES (FIG. 7)

Part No.†	No. of composite layers	Test ultimate load (Kips)	Test elastic buckling load (Kips)	Analysis, buckling prediction	
				Load (Kips)	Ratio test/analysis
11-A	30	180 (0·0048)‡	129 (0·0028)‡	150·8 (0·0033)† (12)§	0·85
11-B	30	210 (0·0056)		154·1 (0·0033) (6)	
11-C	20	155 (0·0052)	30	33·5 (0·00088) (14)	0·90
11-D	20	181 (0·0061)		33·8 (0·00089) (6)	
11-E	20	111 (0·0028)		150·4 (0·0038) (1)	
11-F	20	211 (0·0056)		200·5 (0·0051) (1)	
11-G	70	356 (0·0043)	257 (0·0032)	343·4 (0·0038) (12)	0·75
11-H	70	461 (0·0056)		345·9 (0·0038) (5)	
11-I	70	350 (0·0042)	325 (0·0026)	351·4 (0·0038) (12)	0·93
11-J	70	232 (0·0028)		349·9 (0·0039) (6)	

† All specimens are titanium except 11-A and 11-B which are Al alloy.
‡ Unit Strain, in./in.
§ Axial half-wave number.

among plate and beam elements with offsets and the considerations of the unloaded edges of the structure are consistent with the linear plate theory and elementary beam theory.

Reasonably good agreement with existing analytical and test data is obtained from the results of the correlation study. Some scattering in test correlations indicates the degree of uncertainties in dealing with the composite reinforced stiffened structures. Further complication arises from the uncertain properties of the adhesive layer which bond the composite lamina to the metal. When the thickness of the adhesive layer is of comparable order of magnitude as the thickness of the composites, it could be important to include the elasticity of the adhesive layer and the effect of the inter-lamina shear into the analysis.

Since the present method combines local instability, which involves only some of the elements, as well as general instability, which involves the whole structure, the solution of the eigenvector for the particular eigenvalue (buckling load) is useful. This eigenvector capability has been included and it would be useful in an optimization analysis where the weak members which buckled first could be detected and reinforced.

Acknowledgements—The authors are indebted to M. F. Card and R. A. Pride of Langley Research Center, NASA, for valuable discussions and to S. Oken, V. Oeverli and C. Gagnon of the Boeing Company for test information, programming and numerical analysis support.

REFERENCES

[1] W. RAMBERG and S. LEVY, Instability of extrusions under compressive loads. *J. aeronaut. Sci.* (1945).
[2] S. GOODMAN and E. BOYD, Instability of Outstanding Flanges Simply Supported at One Edge and Reinforced by Bulbs at Other Edge, TN-1433, NACA (1947).
[3] S. GOODMAN, Elastic Buckling of Outstanding Flanges Clamped at One Edge and Reinforced by Bulbs at Other Edge, TN-1985, NACA (1949).
[4] P. C. HU and J. C. MCCULLOCH, The Local Buckling Strength of Lipped Z-Columns with Small Lip Width, TN-1335, NACA (1947).
[5] W. H. WITTRICK, A unified approach to the initial buckling of stiffened panels in compression. *Aeronaut. Q.* **19**, 265–283 (1968).
[6] F. W. WILLIAMS and W. H. WITTRICK, Computational procedures for a matrix analysis of the stability and vibration of thin flat-walled structures in compression. *Int. J. mech. Sci.* **11**, 979–998 (1969).
[7] A. H. CHILVER, A generalized approach to the local instability of certain thin-walled struts. *Aeronaut. Q.* **IV**, 245–260 (1953).
[8] J. H. GOLDBERG, J. L. BOGDANOFF and W. D. GLAUZ, *Lateral and Torsional Buckling of Thin-walled Beams*, Vol. 24, pp. 91–100. IABSE Publications (1964).
[9] P. S. BULSON, Local Stability and Strength of Structural Sections, in *Thin-Walled Structures*, edited by A. H. CHILVER. Chatto and Windus (1967).
[10] P. S. BULSON, The Local Instability of Structural Sections with Flange Reinforcements, in *Thin-Walled Steel Structures*, edited by R. C. ROCKEY. Grosby and Lockwood (1969).
[11] A. A. GHOBARAH and W. K. TSO, Overall and local buckling of channel columns. *J. Engng Mech. Div. Am. Soc. civ. Engrs* **95**, 447–462 (1969).
[12] S. W. TSAI, Strength Characteristics of Composite Materials, CR-224, NASA (1965).
[13] J. E. ASHTON, J. C. HALPIN and P. E. PETIT, *Primer on Composite Materials: Analysis, Progress in Material Sciences*, Vol. III. Technomic Publishing (1969).
[14] V. OEVERLI and A. V. VISWANATHAN, (a) BUCLAP—A Computer Program for Uniaxial Compressive Buckling Loads of Orthotropic Laminated Plates, NASA CR-111869 (1971); (b) BUCLAS—A Computer Program for Uniaxial Compressive Buckling Loads of Orthotropic Laminated Structural Sections, NASA CR-111870 (1971); (c) BUCLASP—A Computer Program for Uniaxial Compressive Buckling Loads of Orthotropic Laminated Stiffened Plates, NASA CR-111871 (1971).
[15] A. V. VISWANATHAN, T. C. SOONG and R. E. MILLER, JR., Buckling Analysis for Axially Compressed Flat Plates, Structural Sections and Stiffened Plates Reinforced with Laminated Composites, NASA CR-1889 (1971).
[16] J. H. ARGYRIS and P. C. DUNNE, *Structural Principles and Data*, edited by D. M. A. LEGGETT and M. LANGLEY. Pitman Press (1934).

[17] R. J. ROARK, *Formulas for Stress and Strain*, 4th edition. McGraw-Hill (1965).
[18] J. P. PETERSON, Structural Efficiency of Aluminum Multiweb Beams and *Z*-Stiffened Panels Reinforced with Filamentary Boron-Epoxy Composite, TN D-5856, NASA (1970): also presented at the *AIAA/ASME 11th Structures, Structural Dynamics and Materials Conf.*, Denver, Colo. (1970).
[19] R. A. PRIDE, D. M. ROYSTER and J. E. GARDNER, Influence of Various Fabrication Methods on the Compressive Strength of Titanium Skin-Stringer Panels, TND-5389, NASA (1969).
[20] H. BECKER, Handbook of Structural Stability, Part II, TN-3782, NACA (1957).
[21] D. L. BLOCK, M. F. CARD and M. M. MIKULAS, JR., Buckling of Eccentrically Stiffened Orthotropic Cylinders, TN D-2960, NASA (1965).
[22] M. S. ANDERSON, Local Instability of the Elements of a Truss-Core Sandwich Plate, TR R-30, Figure 5(a), p. 6, NASA (1959).
[23] Engineering Sciences Data, 01.01.18 and 01.01.20, Engineering Sciences Data Unit, Royal Aeronautical Society, London.
[24] J. F. MANDELL, An Experimental Investigation of the Buckling of Anisotropic Fiber Reinforced Plastic Plates, AFML-TR-68-281 Air Force Materials Laboratory, Wright–Patterson AFB, Ohio (1968).
[25] J. E. ASHTON and T. S. LOVE, Experimental study of the stability of composite plates. *J. Composite Mater.* **3**, 230 (1969).

(*Received* 4 *March* 1971; *revised* 2 *August* 1971)

Абстракт—Даётся классический анализ выпучивания подкреплённых пластинок, сложенных из рядов связанных пластин и балочных элементов. Идеализируются пластинки многослойными ортотропными элементами; рассматриваются борты и края пластинок как балки. Нагруженные края усиленных ребрами пластинок свободно опертые. Усилия на ненагруженных краях произвольные. Пластинка и балочные элементы, вдоль их соединений, подобранные точным способом, с целью исполнения непрерывносности деформаций и условия равновесия усилий.

В анализе учитываются отклонения между элементами. Исследуется выпучивание пластинок, участков и подкреплённых пластинок, пол вдиянием одноосной сжимаемой нагрузки. Определяются нагрузки выпучивания более низкие по сравнению со всеми обще возможными.

Для определения вопроса является ли выпучивание локальной или общей неустойчивостью, используется локальные виды выпучивания. Обсуждаются численные корреляции между предложенным анализом и опытными результатами для пластинок, участков и подкреплённых пластинок, заключая конструкции усиленные бором. Сходимисть корреляции умеренно надлежащая.